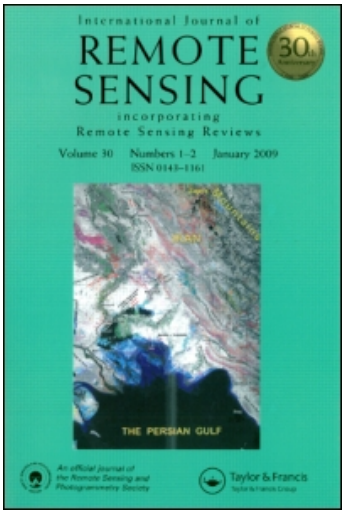

International Journal of Remote Sensing
Publication details, including instructions for authors and subscription information:
http://www.informaworld.com/smpp/title~content=t713722504

Modelling net primary productivity of terrestrial ecosystems in East Asia based on an improved CASA ecosystem model

Deyong Yu [a]; Peijun Shi [a]; Hongbo Shao [bcd]; Wenquan Zhu [a];Yaozhong Pan [a]
[a] State Key Laboratory of Earth Surface Processes and Resource Ecology, Key Laboratory of Environment Change and Natural Disaster, MOE/Academy of Disaster Reduction and Emergency Management, Beijing Normal University, Beijing, China [b] State Key Laboratory of Soil Erosion and Dryland Farming on the Loess Plateau, Institute of Soil and Water Conservation, Chinese Academy of Sciences, Yangling, China [c] Yantai Institute of Coastal Zone Research for Sustainable Development, Chinese Academy of Sciences (CAS), Yantai, China [d] Institute of Life Sciences, Qingdao University of Science and Technology, Qingdao, China

To cite this Article Yu, Deyong , Shi, Peijun , Shao, Hongbo , Zhu, Wenquan andPan, Yaozhong(2009) 'Modelling net primary productivity of terrestrial ecosystems in East Asia based on an improved CASA ecosystem model', International Journal of Remote Sensing, 30: 18, 4851 — 4866
To link to this Article: DOI: 10.1080/01431160802680552
URL: http://dx.doi.org/10.1080/01431160802680552

International Journal of Remote Sensing
Vol. 30, No. 18, 20 September 2009, 4851–4866

Taylor & Francis
Taylor & Francis Group

Modelling net primary productivity of terrestrial ecosystems in East Asia based on an improved CASA ecosystem model

DEYONG YU*†, PEIJUN SHI†, HONGBO SHAO‡, WENQUAN ZHU† and YAOZHONG PAN†

†State Key Laboratory of Earth Surface Processes and Resource Ecology, Key Laboratory of Environment Change and Natural Disaster, MOE/Academy of Disaster Reduction and Emergency Management, Beijing Normal University, Beijing 100875, China

‡State Key Laboratory of Soil Erosion and Dryland Farming on the Loess Plateau, Institute of Soil and Water Conservation, Chinese Academy of Sciences, Yangling 712100, China; Yantai Institute of Coastal Zone Research for Sustainable Development, Chinese Academy of Sciences (CAS), Yantai 264003, China; Institute of Life Sciences, Qingdao University of Science and Technology, Qingdao 266042, China

(*Received 20 September 2006; in final form 8 February 2008*)

By using a land cover map, normalized difference vegetation index (NDVI) data sets, monthly meteorological data and observed net primary productivity (NPP) data, we have improved the method of estimating light use efficiency (LUE) for different biomes and soil moisture coefficients in the Carnegie–Ames–Stanford Approach (CASA) ecosystem model. Based on this improved model we produced an annual NPP map (in 1999) for the East Asia region located at 10–70° N, 70–170° E (about 19.66% of the terrestrial surface of the Earth). The results show that the mean NPP for the study area in 1999 was 374.12 g carbon (C) m^{-2} $year^{-1}$ and the total NPP was 1.096×10^{14} kg C $year^{-1}$, making up 17.51–18.39% of the global NPP. Comparison between the estimated NPP obtained from this improved CASA ecosystem model and the observed NPP obtained from two NPP databases indicates that the estimated NPP is close to the observed NPP, with an average error of 5.15% for the study region. We used two different land cover maps of China to drive the improved CASA model by keeping other inputs unchanged to determine how the classification accuracy of the land cover map affects the estimated NPP, and the results indicate that an accurate land cover map is important for obtaining an accurate and reliable estimate of NPP for some regions, especially for a particular biome.

1. Introduction

Net primary productivity (NPP), an indicator reflecting the extent of vegetation utilization in natural conditions, is the dry matter produced by green vegetation per unit area and per unit time (Peng *et al*. 2000). Spatiotemporal variation in NPP is mainly affected by the complex interaction between vegetation, soil and climate factors, and is also strongly affected by human activities. NPP is a sensitive indicator of climate and environmental changes (Schimel *et al*. 1995). Although there are many uncertainties in estimating NPP on a large scale, it is currently very important to estimate NPP in order to determine the evolution of terrestrial ecosystems, and study

*Corresponding author. Email: dyyucas@163.com

International Journal of Remote Sensing
ISSN 0143-1161 print/ISSN 1366-5901 online
http://www.tandf.co.uk/journals
DOI: 10.1080/01431160802680552

the response of the ecosystems to climate change (Field *et al*. 1995, Cramer *et al*. 1999). There are many models for estimating NPP. Ruimy and Saugier (1994) generalized these models into three categories: (1) statistical-, (2) parameter- and (3) process-based models. The Carnegie–Ames–Stanford Approach (CASA) ecosystem model based on estimating light use efficiency (LUE) is a process-based model appropriate for the estimation of NPP on a global or regional scale. LUE means the efficiency that vegetation translates photosynthetically active radiation into organic carbon. LUE directly affects energy distribution, and one of the key topics in estimating NPP based on the CASA ecosystem model is the correct estimation of LUE. Potter *et al*. (1993) stated that vegetation has a maximal LUE in ideal conditions but is easily affected by actual temperature and moisture conditions. Potter *et al*. (1993) and Field *et al*. (1995, 1998) reported that the maximal LUE of different vegetation types in rational conditions should be 0.389 g carbon (C) $(MJ)^{-1}$, and they used the CASA ecosystem model to obtain 4.89×10^{14} kg C for the global terrestrial ecosystem. Jeffrey (2006) set the maximal LUE for different vegetation types in the two data sets from the National Centers for Environment Prediction (NCEP) and the Goddard Institute for Space Studies (GISS) to 0.46 and 0.50 g C $(MJ)^{-1}$, respectively, when he used the CASA model to compare the quality of the two data sets. However, the maximal LUE is affected by temperature, water, soil, nutrition, disease, individual development, gene difference and energy distribution in the real situation (Prince 1991), so it should not be set to a sole value for different vegetations (Goetz and Prince 1996, Paruelo *et al*. 1997, McCrady and Jokela 1998).

In the CASA model, moisture stress coefficients are calculated by the soil moisture model, which is related to many soil parameters such as field moisture capacity, the wilting coefficient, the percentage of soil sand and clay particles, and the depth of the soil. In general, these soil parameters are extracted from a soil class map whose accuracy is low on a large geographical scale and it is difficult to obtain them.

Due to the limitations of the CASA model, we aimed to improve the model from the two aspects: (1) according to the principle of minimal error between the estimated NPP and observed NPP (field measurement data), we constructed an equation to model the maximal LUE for different vegetation types; (2) by excluding several soil parameters, we used monthly meteorological data (monthly total solar radiation, monthly average temperature and monthly total precipitation) and referred to the existing regional evapotranspiration model to estimate regional moisture stress coefficients. This treatment not only keeps the plant physiological and ecological basis of the original CASA ecosystem model but also simplifies the input parameters.

2. The improved CASA ecosystem model

In the CASA ecosystem model, the product of absorbed photosynthetically active radiation (APAR) and LUE was used to define NPP as in equation (1) (Potter *et al*. 1993):

$$N(x,t) = A(x,t) \times \varepsilon(x,t) \tag{1}$$

where $N(x, t)$ represents the NPP in the geographic coordinate system of a given location x and time t. $A(x, t)$ (MJ m^{-2}/month) means the APAR by the vegetation. $\varepsilon(x, t)$ is the LUE (g C $(MJ)^{-1}$) of the vegetation. A flow chart of the improved CASA algorithm used to produce the NPP is shown in figure 1.

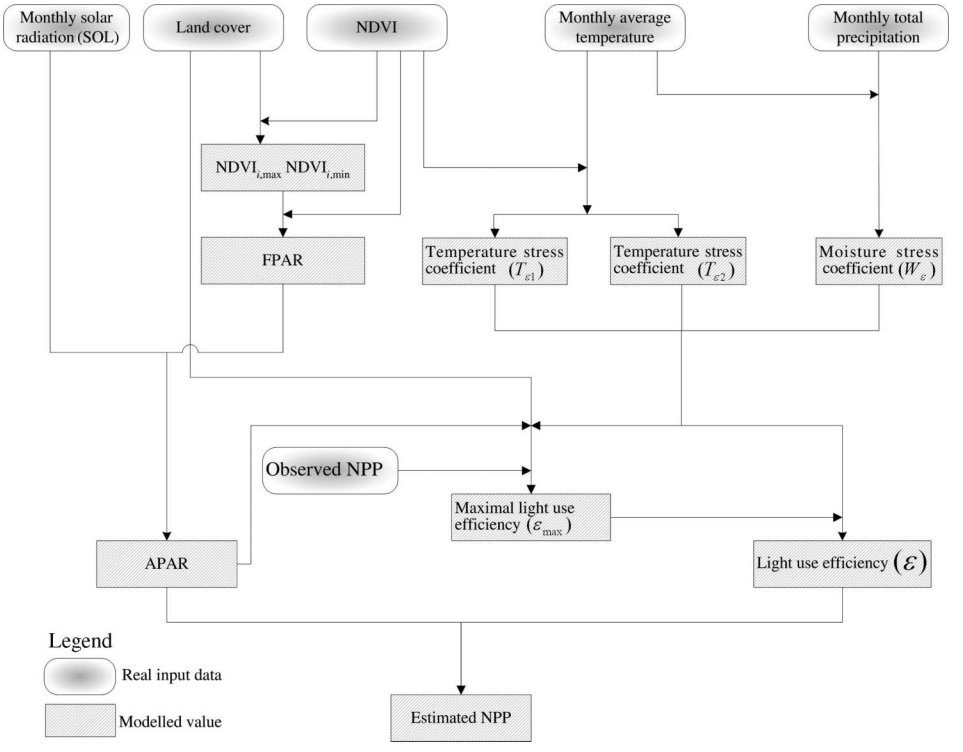

Figure 1. The improved NOAA-AVHRR productivity logic has three key components: (1) remote sensing inputs (land cover, NDVI), (2) monthly surface weather inputs, (monthly solar radiation (SOL), which is used to estimate APAR; monthly average temperature and monthly total precipitation, which are used to estimate temperature stress coefficients ($T_{\varepsilon 1}$, $T_{\varepsilon 1}$) and moisture stress coefficient (W_{ε})), and (3) a look-up table containing biome-specific coefficients (observed NPP, ε_{max} and ε). Based on the land cover, observed NPP, temperature stress coefficients and moisture stress coefficient, a characteristic radiation conversion efficiency parameter (ε_{max}) is extracted to produce ε, which is then used with the Absorbed Photosynthetic Active Radiation (APAR) to predict the monthly NPP [$N(x,t) = A(x,t) \times \varepsilon(x,t)$, where $A(x,t) = S(x,t) \times F(x,t) \times r$ and r is the ratio of the solar radiation (with wavelength range of 0.38–0.71 μm) that can be used by the vegetation to the total solar radiation]. The final estimation of the annual NPP is obtained by adding the 12-month NPP in a year.

2.1 *Estimation of APAR*

The algorithm of APAR is given by equation (2) (Piao *et al.* 2001):

$$A(x,t) = S(x,t) \times F(x,t) \times r \tag{2}$$

where $S(x,\ t)$ (MJ m^{-2}/month) is the monthly total solar radiation, $F(x,\ t)$ is the fraction of photosynthetically active radiation (FPAR) at position x and time t, and r is the ratio of the solar radiation (with a wavelength range of 0.38–0.71 μm) that can be used by the vegetation with the total solar radiation ($r \approx 0.5$) (Piao *et al.* 2001). FPAR is mainly determined by vegetation type and its canopy. The normalized difference vegetation index (NDVI), calculated by remote sensed data, is used to reflect the vegetation canopy (Potter *et al.* 1993). The relationship between FPAR and

NDVI is nearly linear and has been defined by equation (3) (Sellers 1985, Huemmrich and Goward 1992, Potter *et al.* 1993, Ruimy and Saugier 1994):

$$F(x,t) = \frac{[(\mathrm{NDVI})(x,t) - (\mathrm{NDVI})_{i,\min}] \times (F_{\max} - F_{\min})}{\mathrm{NDVI}_{i,\max} - \mathrm{NDVI}_{i,\min}} + F_{\min} \tag{3}$$

$F_{\min}$ (= 0.001) and $F_{\max}$ (= 0.95), the minimal and maximal FPAR, respectively, are independent of vegetation type. $(\mathrm{NDVI})_{i,\min}$ and $(\mathrm{NDVI})_{i,\max}$ are the statistical minimal and maximal NDVI values of vegetation type i and represent bare and full cover with the vegetation type i, respectively. The algorithm of $(\mathrm{NDVI})_{i,\min}$ can be described by the following two steps: (1) at an interval of 0.0001, calculate the minimal NDVI probability distribution of all pixels of vegetation type i; (2) the NDVI value corresponding to the fifth percentile of the distribution is selected as $(\mathrm{NDVI})_{i,\min}$. Similarly, the algorithm of $(\mathrm{NDVI})_{i,\max}$ can be calculated: (1) at an interval of 0.0001, calculate the maximal NDVI probability distribution of all pixels of vegetation type i; (2) the NDVI value corresponding to the 95th percentile of the distribution is selected as $(\mathrm{NDVI})_{i,\max}$.

Some studies have indicated that FPAR is also linearly related to a simple ratio (SR) that can be expressed as a transformation of NDVI. The linear relationship of FPAR and SR can be expressed by equation (4) (Los *et al.* 1994, Field *et al.* 1995, Sellers *et al.* 1996):

$$F(x,t) = \frac{[D(x,t) - D_{i,\min}] \times (F_{\max} - F_{\min}}{D_{i,\max} - D_{i,\min}} + F_{\min} \tag{4}$$

where $D(x,\ t)$ represents the SR and $D(x,t) = \frac{1+(\mathrm{NDVI})(x,t)}{1-(\mathrm{NDVI})(x,t)}$. $D_{i,\min}$ and $D_{i,\max}$ are calculated using $(\mathrm{NDVI})_{i,\min}$ and $(\mathrm{NDVI})_{i,\max}$ as the values for the NDVI, respectively.

The comparison indicated a larger and smaller bias than the field observed value in estimating FPAR through NDVI and SR, respectively. However, the error estimated through SR is smaller than through NDVI. Los (1998) found the smallest error with the field observed value in estimating FPAR from the mean value estimated by NDVI and SR, respectively, and gave the integrated model as in equation (5):

$$F(x,t) = \alpha F_1 + (1-\alpha)F_2 \tag{5}$$

where F_1 and F_2 are FPAR calculated by equations (3) and (4), respectively, and α is set to 0.5.

2.2 *Estimation of LUE*

The algorithm of LUE can be expressed by equation (6):

$$\varepsilon(x,t) = T_{\varepsilon 1}(x,t) \times T_{\varepsilon 2}(x,t) \times W_{\varepsilon}(x,t) \times \varepsilon_{\max} \tag{6}$$

where $\varepsilon(x,\ t)$ is the LUE, $T_{\varepsilon 1}(x,\ t)$ and $T_{\varepsilon 2}(x,\ t)$ are temperature stress coefficients, W_{ε} $(x,\ t)$ is the moisture stress coefficient, and $\varepsilon_{\max}$ is the maximal LUE of the vegetation in ideal conditions.

2.2.1 Estimation of temperature stress coefficients. $T_{\varepsilon 1}(x,\ t)$ indicates the restricted extent of extreme low and high temperature conditions to vegetation photosynthesis. $T_{\varepsilon 2}(x,\ t)$ expresses the decreasing trend of LUE of the vegetation when the environment conditions change from the optimal temperature to a lower or higher temperature. The algorithms for $T_{\varepsilon 1}(x,\ t)$ and $T_{\varepsilon 2}(x,\ t)$ have been described by Potter *et al.* (1993) and Field *et al.* (1995).

2.2.2 Estimation of the moisture stress coefficient. W_ε (x, t) shows the effect of effective moisture that can be used by vegetation on LUE. With effective moisture increase, $W_\varepsilon(x, t)$ gradually increases and ranges from 0.5 (in extremely dry conditions) to 1 (in extremely moist conditions). $W_\varepsilon(x, t)$ can be calculated by equation (7) (Piao *et al*. 2001):

$$W_\varepsilon(x,t) = 0.5 + 0.5 \times [E(x,t)/P(x,t)] \tag{7}$$

where $E(x, t)$ is the estimated evapotranspiration and $P(x, t)$ is the potential evapotranspiration. When P (monthly total precipitation) $> P(x, t)$, then $E(x, t) = P(x, t)$; that is $W_\varepsilon(x, t) = 1$. At $P \leq P(x, t)$, $E(x, t)/P(x, t)$ is defined as the regional moisture index to reflect soil moisture, and in this case $E(x, t)$ can be calculated by the evapotranspiration model (equation (8)) (Zhou and Zhang 1995):

$$E(x,t) = \{P \times R(x,t) \times [P^2 + (R(x,t))^2 + P \times R(x,t)]\}/\{[P + R(x,t)] \times [P^2 + R(x,t)^2]\} \tag{8}$$

In equation (8), $R(x, t)$ expresses the net solar radiation in time t (MJ m^{-2}/month). $P(x, t)$ can be calculated using equation (9) (Thornthwaite 1948, Chang 1989, Zhang 1990, Zhou and Zhang 1996):

$$P(x,t) = [E(x,t) + E_0(x,t)]/2 \tag{9}$$

where $E_0(x,t) = 16 \times [10 \times T(x,t)/I(x)]^{\alpha(x)}$. $\alpha(x)$ and $I(x)$ can be calculated by equation (10):

$$\alpha(x) = (0.675I(x)^3 - 77.1I(x)^2 + 17920I(x) + 492390\times10^{-6} \tag{10}$$

where $I(x) = \sum_{i=1}^{12} [T(x,t)/5)]^{1.514}$. $I(x)$ is the total heat index in a year and the expression is true only when the air temperature ranges from 0°C to 26.50°C. $T(x, t)$ is the temperature. When the air temperature is < 0°C, Thornthwaite (1948) set $P(x, t)$ to zero. When the air temperature is > 26.50°C, $P(x, t)$ increases with air temperature and thus is not affected by the value of $I(x)$. In this case, $P(x, t)$ should be calibrated by actual sunshine hours and the number of days in a month as $A_0(x,t) = P(x,t) \times C(x,t)$. $C(x, t)$, when changing at different latitudes, is the coefficient of sunshine hours and number of days in a month (Thornthwaite 1948).

2.2.3 Estimation of the maximal light use efficiency. Three steps are required to estimate ε_{max}: (1) computing each pixel of APAR, $T_{\varepsilon 1}(x, t)$, $T_{\varepsilon 2}(x, t)$ and $W_\varepsilon(x, t)$; (2) selecting suitable observed NPP data; (3) building an equation and computing ε_{max} for different vegetation types according to the principle of minimal error between the observed NPP and estimated NPP.

For one vegetation type, the error function, $E(x)$, between the observed NPP, a, and estimated NPP, b, can be expressed by equation (11):

$$E(x) = \sum_{j=1}^{n} [a(x) - b(x)]^2 \tag{11}$$

where j is the number of observed NPP samples (1 – n) for the vegetation type. Equation (11) can also be expressed as:

$$E(x) = \sum_{j=1}^{n} [a(x) - \varepsilon_{\max}(x)M(x)]^2 \tag{12}$$

with $\varepsilon_{\max} \in [l, u]$ and $M(x) = A(x)T_{\varepsilon 1}(x)T_{\varepsilon 2}(x)W_{\varepsilon}(x)$, where $[l, u]$ is the closed range of the possible $\varepsilon_{\max}(x)$. $M(x)$ can be viewed as a constant and easily computed by the methods described in §§2.1, 2.2.1 and 2.2.2.

Equation (12) can be expanded as:

$$E(x) = \sum_{j=1}^{n} \varepsilon_{\max}(x)^2 M(x)^2 - 2\sum_{j=1}^{n} \varepsilon_{\max}(x)M(x)a(x) + \sum_{j=1}^{n} a(x)^2 \tag{13}$$

Since equation (13) is a one degree and quadratic equation with an upward opening, it must have a minimal value between the closed ranges of $[l, u]$. In this case, the error between the observed NPP and estimated NPP is minimal and $\varepsilon_{\max}$ is just the estimated maximal LUE for the vegetation type.

3. Input requirements for the improved model

3.1 *Remote sensing data*

3.1.1 NDVI data set. The study area spans six temperature zones (tropical zone, subtropical zone, warm temperate zone, mid-temperate zone, cold temperate zone, frigid zone) and is covered with abundant vegetation types. Although spatial resolution of Landsat Multispectral Scanner (MSS), Landsat Thematic Mapper (TM) and SPOT high-resolution visible (HRV) data is relatively high, their revisiting periods are relatively long and do not meet the need of estimating monthly NPP and dynamically monitoring NPP for a large geographical region. In addition, relatively high spatial resolution tends to accentuate specific features and ignore macroscopical rules. National Oceanic and Atmospheric Administration, Advanced Very High Resolution Radiometer (NOAA/AVHRR) data have the characteristics of global cover, a short revisiting period and spatial-temporal continuity, so they are the most effective data sources for studying vegetation, climate and land surface changes (Hansen *et al.* 2000). The NOAA/AVHRR NDVI images with an original spatial resolution of 8 km × 8 km came from the Pathfinder Data Set, which is a product of eliminating cloud contamination and conducting atmosphere calibration developed by the Earth Resources Observation System (EROS). The monthly maximal value composite (MVC) NDVI data were taken from January to December in 1999. The spatial resolution of the NDVI images was finally transformed into 0.075° × 0.075° with the geographic (latitude/longitude) projection.

3.1.2 Land cover map. Land cover maps are mainly used to estimate the fraction of photosynthetically active radiation and the maximal LUE. A land cover map with a spatial resolution of 8 km developed by the University of Maryland (UMD; http://glcf.umiacs.umd.edu/data/landcover/) has a global scope and is appropriate for acquiring the parameters needed to estimate the NPP in the East Asia region. The map classifies land cover in the East Asia region into 13 types: (1) evergreen needleleaf forest (ENF); (2) evergreen broadleaf forest (EBF); (3) deciduous needleleaf forest (DNF); (4) deciduous broadleaf forest (DBF); (5) mixed forest (MF); (6) woodland (WL); (7) wooded grassland (WG); (8) closed shrubland (CS); (9) open shrubland (OS); (10) grassland (GL); (11) cropland (CL); (12) sparse vegetation (SV); and (13)

tundra vegetation (TV). Although we have corrected some areas of China in the UMD land cover map according to Chinese ground investigation information, the accuracy of the map cannot be greatly improved and the sites used to train the classification algorithm are mostly distributed over the North American Continent, so there may be some questions about its reliability when using the land cover map in the East Asia region to estimate NPP.

We have another land cover map of China with a spatial resolution of 1 km, which was provided by the Joint Research Centre (JRC, The European Union) and was compiled by the Institute of Remote Sensing Application, Chinese Academy of Science. The original remote sensing data used by the land cover map were from SPOT-VGT in 2000 and the field investigation data show that its total classification accuracy was 61.8%. The 22-biome land cover in the map includes needleleaf deciduous forest, needleleaf evergreen forest, broadleaf evergreen forest, broadleaf deciduous forest, bush sparse woods, seaside wet lands, alpine and subalpine meadow, slope grassland, plain grassland, desert grassland, meadow, city, river, lake, swamp, glacier, bare rock, gravel, desert, farmland, alpine and subalpine plain grass.

The two land cover maps were transformed into $0.075^\circ \times 0.075^\circ$ with the geographic (latitude/longitude) projection. We use the UMD and JRC land cover maps to compare the impact of different land cover classification accuracy on estimating NPP.

3.2 *Monthly meteorological data*

The meteorological data required for inputting of the improved CASA ecosystem model include the monthly average air temperatures, monthly total precipitation and monthly total solar radiation in 1999. These data with a spatial resolution of $0.5^\circ \times 0.5^\circ$ were developed by the National Center for Atmospheric Research (NCAR, USA). These gridded data were bilinearly interpolated for each pixel of $0.075^\circ \times 0.075^\circ$ to match NDVI data sets and their projection types are also geographic (latitude/longitude).

3.3 *Selecting the observed NPP from NPP databases*

The observed NPP data were mainly compiled from two NPP databases. One was provided by the Oak Ridge National Laboratory Distributed Active Archive Center on their website (http://www-eosdis.ornl.gov/NPP/npp_home.html). The other one was provided by the former Ministry of Forestry of China and relates to six major forest biomes, includes 690 terrestrial observed sites that lay out 17 forest types in China and geographically pass across the north temperate zone in northeast China to the tropical regions in southern China. Latitude, longitude, elevation, leaf area index, total biomass, and total NPP are documented for each observed site. From these NPP data sources, we obtained observed NPP for several countries and vegetation types (shown in table 1).

4. Results and discussion

4.1 *The maximal LUE (ε_{max}) for different vegetation types*

Table 2 shows the estimated $\varepsilon_{\max}$ for different vegetation types. Due to the lack of observed NPP data for close shrubland, open shrubland, sparse vegetation and tundra, their maximal LUE values were set equal to that of temperate zone grassland. The mean observed NPP and the product APAR $\times$ $T_{\varepsilon 1}$ $\times$ $T_{\varepsilon 1}$ $\times$ W_{ε} for temperate

Table 1. Numbers of study sites obtained from field-measurement NPP databases.

Country	ENF	EBF	DNF	DBF	MF	WL	WG	CS	OS	GL	CL	SV	TV	Total
China	67	120	20	305	18	–	–	–	–	1	1	–	–	532
Japan	10	–	7	5	2	–	–	–	–	–	2	–	–	26
India	–	5	–	–	–	–	–	–	–	10	1	–	–	16
Russia	30	–	8	40	3	–	–	–	–	1	–	–	–	82
Malaysia	–	6	–	–	–	–	–	–	–	–	1	–	–	7
Thailand	–	8	–	–	–	–	–	–	–	–	–	–	–	8
Total	107	139	35	350	23	–	–	–	–	12	5	–	–	671

grassland were 230.6 ± 64.9 g C m^{-2} year^{-1} (Fan *et al*. 2003) and 427.7 MJ m^{-2} year^{-1}, respectively. ε_{max} for the four vegetation types was set to 0.541 g C (MJ)$^{-1}$. ε_{max} of woodland was obtained from the mean value [0.572 g C (MJ)$^{-1}$] for closed shrubland and woodland. ε_{max} of wooded grassland was obtained from the mean value [0.557 g C (MJ)$^{-1}$] for woodland and closed shrubland. Although ε_{max} of close shrubland, open shrubland, sparse vegetation, tundra, woodland and wooded grassland was obtained from other vegetation types because of lack of observed NPP, this does not affect the applicability of the simulation method of ε_{max}. In other words, the number of observed NPP sites is very important for an accurate simulation of ε_{max} if the observed NPP represents the mean quality of the vegetation type.

4.2 *Annual NPP*

The spatial distribution of the NPP over the East Asia region in 1999 and the statistical results are shown in figure 2 and table 3, respectively. The mean NPP over the study area was 374.12 g C m^{-2} year^{-1} in 1999. The mean NPP of evergreen broadleaf forest (1215.82g C m^{-2}) was the largest, followed by that of deciduous broadleaf forest (567.90 g C m^{-2}), cropland (524.66 g C m^{-2}), wooded grassland (445.94 g C m^{-2}), woodland (409.38 g C m^{-2}), mixed forest (407.00g C m^{-2}), evergreen needleleaf forest (330.38 g C m^{-2}), deciduous needleleaf forest (298.25 g C m^{-2}), closed shrubland (266.39 g C m^{-2}), tundra vegetation (243.39 g C m^{-2}), grassland (228.12 g C m^{-2}), and open shrubland (144.14 g C m^{-2}). The mean NPP of sparse vegetation (26.2 g C m^{-2}) was the smallest. Climate conditions in the evergreen broadleaf forest distribution region are suitable for perennial vegetation growth, so its mean NPP was higher. Cultivation measures help to increase the yield of croplands, so the mean NPP of cropland was also higher. Although the growth period of tundra vegetation is relatively short, its mean NPP was higher than that of grassland and open shrubland. Figure 2 showed that the mean NPP of many regions in the south area of 30° N was larger than in the north area. The Tibetan Plateau and Taklimakan desert are low value regions of the mean NPP in the study area. This spatial NPP distribution pattern is in accordance with that of Bunkei and Masayuki (2002), who estimated the NPP for the East Asia region at latitude 66° N–9° S and longitude 78–170° E.

The area of our study region comprises about 19.66% of the global terrestrial area, and the total NPP in 1999 was about 1.096×10^{14} kg C year^{-1}, with 17.51–18.39% of the global total NPP [$(5.96–6.26) \times 10^{14}$ kg C was reported by the Intergovernmental Panel on Climate Change (IPCC) in the third NPP estimation]. Forests (including evergreen needleleaf forest, evergreen broadleaf forest, deciduous needleleaf forest

Table 2. The maximal light use efficiency (ε_{max}) for different vegetation types.

Land cover	Number of samples	ε_{max} (g C (MJ)$^{-1}$)			Mean observed NPP (g C m^{-2} year^{-1})	Range of observed NPP (g C m^{-2} year^{-1})
		Minimum value	Maximum value	Simulated value		
Evergreen needleleaf forest	35	0.210	1.721	0.389	395	179–806
Evergreen broadleaf forest	107	0.168	2.498	0.978	1015	407–1913
Deciduous needleleaf forest	350	0.225	1.970	0.492	678	191–1669
Deciduous broadleaf forest	141	0.461	2.254	0.664	469	179–824
Mixed forest	21	0.237	0.743	0.49	472	257–717
Woodland				0.572		
Wooded grassland				0.557		
Closed shrubland				0.541		
Open shrubland				0.541		
Grassland	12	0.268	0.638	0.541	230.6	192–289
Cropland	5	0.336	0.735	0.608	532.9	152–684
Sparse vegetation				0.541		
Tundra vegetation				0.541		

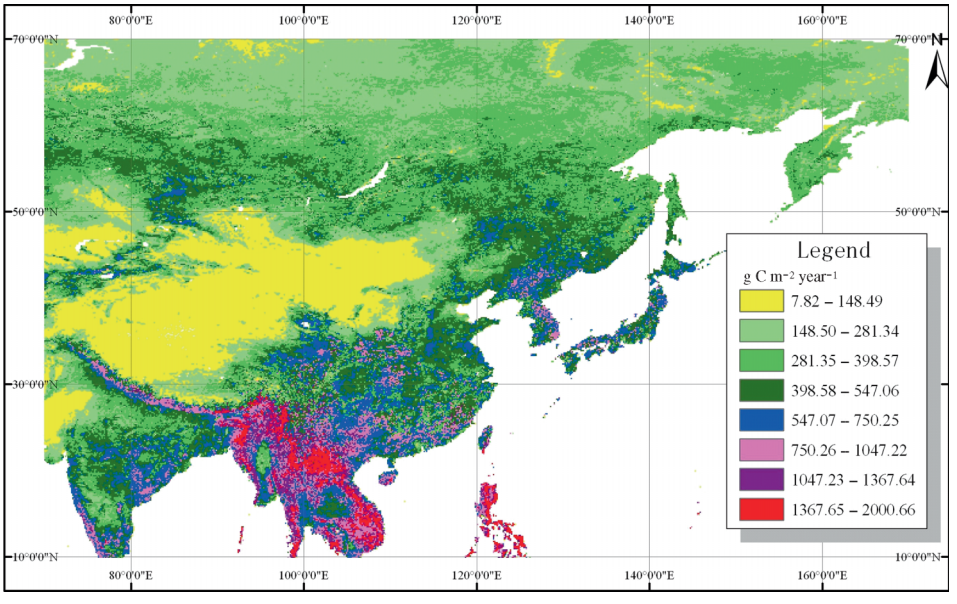

Figure 2. Distribution map of the annual NPP in East Asia, 1999.

Table 3. Mean and total estimated NPP of different vegetation types for the study area in 1999.

Land cover type	Area (10^4 km^2)	Number of pixels	Mean NPP (g C m^{-2} year^{-1})	Total of NPP (10^{13} kg C m^{-2} year^{-1})	Percentage of area (%)	Percentage of NPP (%)
ENF	379.46	59290	330.38	1.25	12.95	11.44
EBF	151.78	23716	1215.82	1.85	5.18	16.84
DNF	245.48	38357	298.25	0.73	8.38	6.68
DBF	121.58	18997	567.90	0.69	4.15	6.30
MF	161.08	25168	407.00	0.66	5.50	5.98
WL	219.93	34364	409.38	0.90	7.51	8.21
WG	168.04	26257	445.94	0.75	5.74	6.84
CS	34.07	5324	266.39	0.09	1.16	0.83
OS	151.01	23595	144.14	0.22	5.15	1.99
GL	569.96	89056	228.12	1.30	19.46	11.86
CL	360.87	56386	524.66	1.89	12.32	17.27
SV	119.26	18634	26.20	0.03	4.07	0.29
TV	247.03	38599	243.39	0.60	8.43	5.49
Whole study area	2929.55	457743	374.12	10.96	100.00	100.00

and deciduous broadleaf forest) comprise 36.16% of the study area, and the forest NPP makes up 47.23% of the total NPP of the study area. Forest areas and their total NPP percentages are approximately in accordance with the results of Bunkei and Masayuki (2002), in which the forests (including broadleaf and needleleaf forests) comprise just 32% of the East Asia region and the forest NPP makes up 45% of the total NPP of the East Asia region.

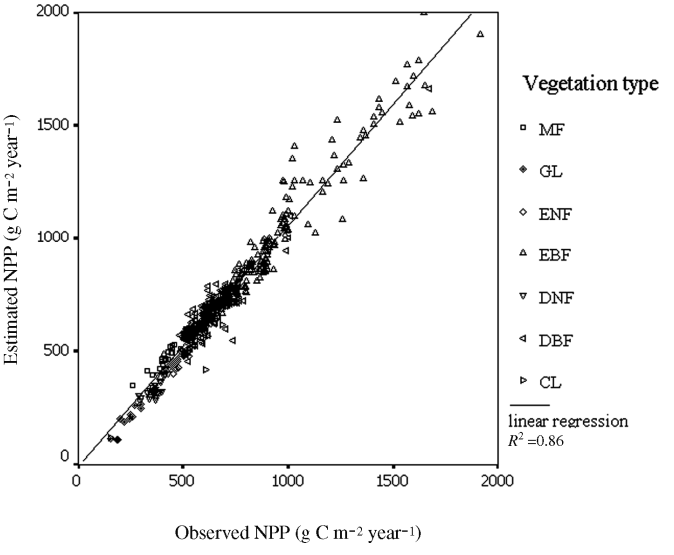

Figure 3. Comparison of the estimated and observed NPP in the East Asia area. The average errors for CL, DBF, DNF, EBF, ENF, GL and MF were 13.91, 6.17, –6.21, 7.24, –6.56, –15.47 and 13.3%, respectively, and the average total error of the seven-biome land cover was found to be 5.15%.

The total NPP of crops (1.89×10^{13} kg C year^{-1}) was the largest, followed by that of evergreen broadleaf forest (1.85×10^{13} kg C year^{-1}), grassland (1.3×10^{13} kg C year^{-1}), evergreen needleleaf forest (1.25×10^{13} kg C year^{-1}), woodland (0.9×10^{13} kg C year^{-1}), wooded grassland (0.75×10^{13} kg C year^{-1}), deciduous needleleaf forest (0.73×10^{13} kg C year^{-1}), deciduous broadleaf forest (0.69×10^{13} kg C year^{-1}), mixed forest (0.66×10^{13} kg C year^{-1}), tundra vegetation (0.60×10^{13} kg C year^{-1}), open shrubland (0.22×10^{13} kg C year^{-1}), and closed shrubland (0.09×10^{13} kg C year^{-1}). The total NPP of sparse vegetation (0.03×10^{13} kg C year^{-1}) was the smallest.

A scatter plot of the observed and estimated NPP is shown in figure 3. This figure indicates that the estimated results in the total are reasonable and can be accepted with an average error of 5.15% between the observed and estimated NPP. It should be pointed out that the average error is due to the offsets of positive and negative errors, and the errors of estimated total NPP for each vegetation type ranged from –15.47% to 13.91% (figure 3). The reasons may be that: (1) vegetation type in the UMD map may be misclassified; (2) the accuracy of other inputs such as meteorological and remotely sensed data may result in errors in the estimated NPP; (3) low numbers of representative observed NPP sample sites for biomes may cause errors in the estimated NPP; and (4) even though the CASA ecosystem model at the stand level has been developed in great detail, the difference in mechanisms between the model and natural ecosystem may cause problems when using the model on a large geographical scale. In addition, the precision of the estimated NPP outside of the observed sites should be further verified by collecting observed NPP in future work.

4.3 *Evaluating the effect of land cover map accuracy on the estimated NPP*

There are some differences of classification standards between the two land cover maps. Casually combining the classes may cause subjective errors, so we selected

six-biome land covers of evergreen needleleaf forest, evergreen broadleaf forest, deciduous needleleaf forest, deciduous broadleaf forest, grassland (including alpine and subalpine meadow, slope grassland, plain grassland, desert grassland, and meadow in the JRC map) and cropland to study the effect of classification accuracy on the estimated NPP.

We used the two independent land cover maps (the China part in the UMD map and the JRC map) to drive the improved CASA model and estimate the Chinese NPP, with other input data and parameters unchanged. We assumed that the classification of the UMD land cover map was correct. The estimated results by the two land cover maps are shown in table 4. According to this table, compared with using the UMD land cover map, use of the JRC land cover map resulted in underestimation of the total NPP in evergreen needleleaf forest (24.15%), evergreen broadleaf forest (22.53%) and cropland (15.06%) and overestimation in deciduous needleleaf forest (307.35%), deciduous broadleaf forest (9.81%) and grassland (35.4%). The error of total deciduous needleleaf forest NPP is the largest (307.5%). The total NPP error of the six-biome land covers in China is at an acceptable level (–2.60%) because of the offsets of positive and negative errors.

A comparison of the JRC land cover map with the UMD land cover map in China is shown in table 5. The numbers in parentheses are percentages of the total pixels of the UMD map in the JRC map and in each class. The italicized numbers indicate the correct classification for each class, and the remainders indicated misclassification. The percentage of correct classification changed from 0 to 52% (table 5). The percentage of misclassification of deciduous needleleaf forest is the highest and it was completely misclassified in the JRC land cover map compared with the UMD land cover map, in which it was mainly classified into evergreen needleleaf forest (44%) and evergreen broadleaf forest (27%). Only 4% of deciduous needleleaf forest in the JRC land cover map was correct by comparison to that in the UMD land cover map. This indicates that the largest error in total estimated NPP for deciduous needleleaf forest is mainly caused by misclassification. In general, the classification error of a land cover map based on remotely sensed data should be less than 40% on a large geographical scale. Therefore, the 307.35% of error in NPP estimation for deciduous needleleaf forest cannot be accepted; it should also be less than 40%. The difference of classification accuracy between the different land cover maps might be very large and using only limited training sites distributed over Europe or the North American Continent is not sufficient for development of a correct algorithm in China. On a continental or global scale, training sites used to classify land covers should be chosen by fully considering the spatial difference and the characteristics of all biomes.

The results shown in tables 4 and 5 indicate that the accuracy of the land cover map is very important to estimate NPP more accurately and reliably for some regions, and this is especially true for a particular biome. Furthermore, an accurate and reliable land cover map can greatly reduce the uncertainty of the model.

5. Conclusion

Using a land cover map, NDVI data sets, monthly meteorological data and observed NPP data, we improved the CASA ecosystem model in two aspects: (1) ignoring most soil parameters and estimating the moisture stress coefficient based on the regional moisture index (the ratio of regional actual evapotranspiration with potential evapotranspiration), which can preferably reflect regional moisture conditions and be

Table 4. Comparison of NPP estimated by using an UMD land cover map and a JRC land cover map of China.

	Estimated NPP based on UMD land cover map				Estimated NPP based on JRC land cover map				
Land cover type	Area (10^4 km^2)	Number of pixels	Mean NPP (g C m^{-2} year^{-1})	Total NPP (10^{13} kg C year^{-1})	Area (10^4 km^2)	Number of pixels	Mean NPP (g C m^{-2} year^{-1})	Total NPP (10^{13} kg C year^{-1})	Error (%)*
ENF	113.82	17 784	390.90	0.44	91.29	14 264	369.66	0.34	−24.15
EBF	50.00	7812	982.68	0.49	40.13	6271	948.36	0.38	−22.53
DNF	4.84	756	426.64	0.02	19.76	3088	425.48	0.08	307.35
DBF	40.09	6264	622.58	0.25	45.16	7057	606.82	0.27	9.81
GL	281.55	43 992	203.14	0.57	248.47	38 823	311.67	0.77	35.40
CL	185.47	28 980	512.58	0.95	167.13	26 114	483.18	0.81	−15.06
Total	675.76	105 588		2.73	611.95	95 617		2.66	−2.60

*Taking the estimated NPP based on the UMD land cover map as the denominator.

Table 5. Comparison of the land cover classification between JRC and UMD land cover maps.*

	UMD land cover map												
JRC land cover map	ENF	EBF	DNF	DBF	MF	WL	WG	CS	OS	GL	CL	SV	TV
ENF	*540 (18)*	0 (0)	324 (11)	324 (11)	1440 (48)	0 (0)	0 (0)	0 (0)	0 (0)	144 (5)	108 (4)	0 (0)	144 (5)
EBF	5688 (18)	*2520 (17)*	0 (0)	504 (3)	288 (2)	1116 (7)	720 (5)	0 (0)	108 (1)	900 (6)	3204 (21)	0 (0)	0 (0)
DNF	2808 (44)	1728 (27)	*0 (0)*	252 (4)	108 (2)	432 (7)	144 (2)	0 (0)	0 (0)	36 (1)	900 (14)	0 (0)	0 (0)
DBF	1260 (19)	36 (1)	36 (1)	*1944 (29)*	2088 (32)	0 (0)	0 (0)	0 (0)	36 (1)	288 (4)	936 (14)	0 (0)	0 (0)
GL	1692 (17)	108 (1)	0 (0)	288 (3)	144 (1)	432 (4)	324 (3)	432 (4)	792 (8)	*5148 (52)*	288 (3)	144 (1)	108 (1)
CL	900 (21)	684 (16)	0 (0)	180 (4)	0 (0)	144 (3)	144 (3)	72 (2)	396 (9)	324 (7)	*1512 (35)*	0 (0)	0 (0)

*We assumed that the classification of the UMD land cover map was correct. Numbers in parentheses are percentages of the total pixels in each class.The italicized numbers mean the correct classification for each class, and the others indicated misclassification.

conveniently and accurately computed by meteorological data; and (2) according to the principle of minimal error between the estimated NPP and observed NPP, we constructed an equation and obtained the maximal LUE for different biomes but not the sole value [0.389 g C $(MJ)^{-1}$] in the original CASA ecosystem model.

Using this improved CASA ecosystem model, we calculated the annual NPP for the East Asia region in 1999. The mean NPP of sparse vegetation was the smallest (26.2 g C m^{-2} $year^{-1}$), followed by that of open shrubland (144.14 g C m^{-2} $year^{-1}$), grassland (228.12 g C m^{-2} $year^{-1}$), tundra vegetation (243.39 g C m^{-2} $year^{-1}$), closed shrubland (266.39 g C m^{-2} $year^{-1}$), deciduous needleleaf forest (298.25 g C m^{-2} $year^{-1}$), evergreen needleleaf forest (330.38 g C m^{-2} $year^{-1}$), mixed forest (407g C m^{-2} $year^{-1}$), woodland (409.38 g C m^{-2} $year^{-1}$), wooded grassland (445.94 g C m^{-2} $year^{-1}$), cropland (524.66 g C m^{-2} $year^{-1}$), and deciduous broadleaf forest (567.9 g C m^{-2} $year^{-1}$). The mean NPP of evergreen broadleaf forest was the largest (1215.82 g C m^{-2} $year^{-1}$). The errors between the estimated NPP and observed NPP for each vegetation type ranged from –15.47% to 13.91%. Due to the offsets of positive and negative errors, the average error between the observed NPP and estimated NPP is 5.15%.

Compared with the UMD land cover map, the percentage of correct classification in the JRC land cover map changed from 0 to 52%, resulting in underestimation of the total NPP in evergreen needleleaf forest (24.15%), evergreen broadleaf forest (22.53%), cropland (15.06%) and overestimation in deciduous needleleaf forest (307.35%), deciduous broadleaf forest (9.81%) and grassland (35.4%). An accurate land cover map is important for estimating an accurate and reliable NPP, especially for a particular biome.

Acknowledgements

This research was funded by the Programmes of National Natural Science Foundation of China (40801211), the National Science Fund Project for Distinguished Young Scholars of the National Natural Science Foundation of China (No. 40425008) and the Project of State Key Laboratory of Earth Surface Processes and Resources Ecology (070106). We thank the referees and editors whose comments have improved the quality of the manuscript.

References

Bunkei, M. and Masayuki, T., 2002, Integrating remotely sensed data with an ecosystem model to estimate net primary productivity in East Asia. *Remote Sensing of Environment*, **81**, pp. 58–66.

Chang, H.S., 1989, The potential evapotranspiration (PE) index for vegetation and vegetation-climatic classification (II): an introduction to main methods and PEP program. *Acta Phytoecologica et Geobotanica Sinica*, **13**, pp. 197–207.

Cramer, W., Kicklighter, D.W., Bondeau, A., Moore, B., Churkina, C., Nemry, B., Ruimy, A. and Schloss, A.L., 1999, Comparing global models of terrestrial net primary productivity (NPP): overview and key results. *Global Change Biology*, **5**, pp. 1–15.

Fan, J.W., Zhong, H.P., Liang, B., Shi, P.L. and Yu, G.R., 2003, Carbon stock in grassland ecosystem and its affecting factors. *Grassland of China*, **25**, pp. 51–58.

Field, C.B., Behrenfeld, M.J., Randerson, J.T. and Falkowski, P., 1998, Primary production of the biosphere: integrating terrestrial and oceanic components. *Science*, **281**, pp. 237–240.

Field, C.B., Randerson, J.T. and Malmstrom, C.M., 1995, Global net primary production: combining ecology and remote sensing. *Remote Sensing of Environment*, **51**, pp. 74–88.

GOETZ, S.J. and PRINCE, S.D., 1996, Remote sensing of net primary production of boreal forest stands. *Agricultural and Forest Meteorology*, **78**, pp. 149–179.

HANSEN, M.C., DEFRIES, R.S., TOWNSHEND, J.R.G. and SOHLBERG, R., 2000, Global land cover classification at 1 km spatial resolution using a classification tree approach. *International Journal of Remote Sensing*, **21**, pp. 1331–1364.

HUEMMRICH, K.F. and GOWARD, S.N., 1992, Spectral vegetation indices and the remote sensing of biophysical parameters. In *Proceedings of the International Geoscience and Remote Sensing Symposium* (Houston, TX: Institute of Electrical and Electronics Engineers), pp. 1017–1019.

JEFFREY, A.H., 2006, NCEP and GISS solar radiation data sets available for ecosystem modeling: description, differences, and impacts on net primary production. *Global Biogeochemical Cycles*, **19**, pp. 1–18.

LOS, S.O., 1998, Linkages between global vegetation and climate: an analysis based on NOAA advanced very high resolution radiometer data. PhD dissertation, National Aeronautics and Space Administration (NASA).

LOS, S.O., JUSTICE, C.O. and TUCKER, C.J., 1994, A global 1° by 1° NDVI dataset for climate studies derived from the GIMMS continental NDVI data. *International Journal of Remote Sensing*, **15**, pp. 3493–3518.

MCCRADY, R.L. and JOKELA, E.J., 1998, Canopy dynamics, light interception, and radiation use efficiency of selected loblolly pine families. *Forest Science*, **44**, pp. 64–72.

PARUELO, J.M., EPSTEIN, H.E., LAUENROTH, W.K. and BURKEI, C., 1997, ANPP estimates from NDVI for the central grassland region of the United States. *Ecology*, **78**, pp. 953–958.

PENG, S.L., GUO, Z.H. and WANG, B.S., 2000, Use of GIS and RS to estimate the light utilization efficiency of the vegetation in Guangdong, China. *Acta Ecoligica Sinica*, **20**, pp. 903–909.

PIAO, S.L., FANG, J.Y. and GUO, Q.H., 2001, Application of the CASA model to the estimation of Chinese terrestrial net primary productivity. *Acta Phytoecologica Sinica*, **25**, pp. 603–608.

POTTER, C.S., RANDERSON, J.T., FIELD, C.B., MATSON, P.A., VITOUSEK, P.M., MOONEY, H.A. and KLOOSTER, S.A., 1993, Terrestrial ecosystem production: a process model based on global satellite and surface data. *Global Biogeochemical Cycles*, **7**, pp. 811–841.

PRINCE, S.D., 1991, A model of regional primary production for use with coarse resolution satellite data. *International Journal of Remote Sensing*, **12**, pp. 1313–1330.

RUIMY, A. and SAUGIER, B., 1994, Methodology for the estimation of terrestrial net primary production from remotely sensed data. *Journal of Geophysical Research*, **97**, pp. 18515–18521.

SCHIMEL, D., ENTING, I.G., HEIMANN, M., WIGLEY, T.M.L., RAYNAUD, D., ALVES, D. and SEIGENTHALER, U., 1995, CO_2 and the carbon cycle. In *Climate Change 1994, Radiative Forcing of Climate Change and an Evaluation of the IPCC IS92 Emission Scenarios*, J.T. Houghton, L.G. Meira Filho, J.P. Bruce, H. Lee, B.A. Callander and E.F. Haites (Eds.) (Cambridge: Cambridge University Press), pp. 35–71.

SELLERS, P.J., 1985, Canopy reflectance, photosynthesis, and transpiration. *International Journal of Remote Sensing*, **6**, pp. 1335–1371.

SELLERS, P.J., RANDALL, D.A., COLLATZ, J.G., BERRY, J.A., FIELD, C.B., DAZLICH, D.A., ZHANG, C., COLLELO, G.D. and BOUNOUA, L., 1996, A revised land-surface parameterization (SiB2) for atmospheric GCMs. Part 1: Model formulation. *Journal of Climate*, **9**, pp. 676–705.

THORNTHWAITE, C.W., 1948, An approach toward a rational classification of climate. *Geographical Review*, **38**, pp. 57–94.

ZHANG, Z.M., 1990, *Rule and Method of Computing Evapotranspiration* (Chengdu: Chengdu Science and Technology Press).

ZHOU, G.S. and ZHANG, X.S., 1995, Natural vegetation NPP model. *Acta Phytoecologica* Sinica, **19**, pp. 193–200.

ZHOU, G.S. and ZHANG, X.S., 1996, Study on NPP of natural vegetation on China under global climate change. *Acta Phytoecologica Sinica*, **20**, pp. 11–19.